Electrochimica Acta 509 (2025) 145270

Contents lists available at ScienceDirect

Electrochimica Acta

journal homepage: www.journals.elsevier.com/electrochimica-acta

Impact of microelectrode geometry and surface finish on enzymatic biosensor performance

Jian Xu [a,b,c,1], Marco Fratus [b,c,d,1], Ankit Shah [a,b,c,1], James K. Nolan [a,b,c], Jongcheon Lim [a,b,c], Chi Hwan Lee [a,b,c,e,f,*], Muhammad A. Alam [b,c,d,*], Hyowon Lee [a,b,c,*]

[a] Weldon School of Biomedical Engineering, Purdue University, West Lafayette, IN 47907, USA
[b] Center for Implantable Devices, Purdue University, West Lafayette, IN 47907, USA
[c] Birck Nanotechnology Center, Purdue University, West Lafayette, IN 47907, USA
[d] Elmore Family School of Electrical and Computer Engineering, Purdue University, West Lafayette, IN 47907, USA
[e] School of Mechanical Engineering, Purdue University, West Lafayette, IN 47907, USA
[f] School of Materials Engineering, Purdue University, West Lafayette, IN 47907, USA

ARTICLE INFO

Keywords:
Biosensor optimization
Fractal electrodes
Platinum black
Polydimethylsiloxane (PDMS) stamping
Microcontact printing
Mathematical model

ABSTRACT

Food production, environmental protection, biotechnology, and medicine, all depend on biosensors for measuring specific biological molecules. Among biosensors, enzymatic electrochemical biosensors have received particular attention due to their simple operation and enzymes' inherent specificity. Researchers have extensively explored novel materials and biological designs to improve performance (i.e., sensitivity, linearity, limit of detection, and response time). However, in comparison, physical and geometrical design has not received the same attention. To this end, we compared platinum (Pt) microelectrodes with circular or fractal geometry with the same surface area (2D geometry). We also studied the effect of 3D geometry by nanostructuring both circular and fractal microelectrodes via electroplating Pt black. Fractal Pt black microelectrodes displayed the highest current density, charge storage capacity, and sensitivity towards H_2O_2. Next, we immobilized glucose oxidase onto various microelectrode geometries by microcontact stamping. Fractal Pt and Pt black glucose biosensors were 91.7 % and 83.3 % more sensitive than circular counterparts. Circular and fractal Pt black glucose biosensors were 63.0 % and 55.9 % more sensitive than Pt counterparts. Fractal geometry also provided better linearity and limit of detection. We modified enzyme layer thickness through multiple layer stamping and found a trade-off whereby increasing thickness increased sensitivity but also increased response time. Lastly, we developed a COMSOL Multiphysics numerical model to interpret the amperometric data and the impact of physical design on critical parameters. The work here will serve as a guideline for improving enzymatic electrochemical and other biosensors via physical design, which is simpler to modify than material or biological design.

1. Introduction

Biosensors measure specific biological analytes, crucial in sectors like food chemistry, environmental protection, biotechnology, and medical applications [1–5]. Their importance is heightened by the rise of personalized medicine, which demands continuous monitoring of metabolites (e.g., glucose, lactate) and neurotransmitters via wearable or implantable devices [6–9]. These devices must offer high sensitivity, selectivity, dynamic range, and quick response times to effectively manage various disorders [10,11]. For instance, biosensors with ultra-high sensitivity and low limit-of-detection (LOD) are essential for the early detection of cancers and cardiovascular diseases [12–14]. Implanted biosensors with high selectivity and response time can closely monitor ascorbic acid and glutamate, biomarkers of post-surgical and post-traumatic injuries [15–18].

Electrochemical biosensors, prevalent due to their simple operation

* Corresponding authors.
E-mail addresses: lee2270@purdue.edu (C.H. Lee), alam@purdue.edu (M.A. Alam), hwlee@purdue.edu (H. Lee).
[1] These authors contributed equality to this work.

https://doi.org/10.1016/j.electacta.2024.145270
Received 22 July 2024; Received in revised form 17 October 2024; Accepted 20 October 2024
Available online 24 October 2024

and high demand for diabetes management through glucose monitoring [18–23], depend heavily on material, biological, and physical design for optimal performance. Material enhancements include novel conductive and stable materials like carbon nanomaterials [24], metal oxides [25], metallic nanoparticles [26], quantum dots [27], and conductive polymers [28–30]. Biological improvements focus on refining the biorecognition elements and their integration with electrodes, utilizing advanced enzyme immobilization techniques to enhance selectivity and sensor lifespan [31–38].

Among the techniques to enhance sensor performance, physical design is the least explored but offers substantial potential for improving biosensor functionality, especially in wearable and implantable forms [9,39–42]. Key physical parameters include electrode geometry [43], surface morphology [44], thickness [45], and functional layer configuration [46], with innovative designs like fractal electrodes providing improved mass transport and electrochemical kinetics compared to conventional circular designs [47,48]. Fractal designs, inspired by their larger perimeter-to-area ratios, exhibit enhanced sensitivity and lower resistance, advantageous for applications like neurostimulation [49–51]. Despite these investigations of physical design, the impact of 2D and 3D microelectrode geometry, together with enzyme layer thickness, surface finish (i.e., Pt black deposition) on glucose biosensor performance parameters has not yet been systematically quantified.

In this study, we address this gap by evaluating the impact of fractal geometry, nanostructured surface finishes, and enzyme layer thickness on the performance of enzymatic biosensors. While our previous research has explored the electrochemical properties of fractal electrodes for delivering charges for neuromodulation study [49], this study is the first to systematically investigate their effects in the context of enzymatic biosensors. Specifically, we compare circular and fractal microelectrodes with smooth or Pt black-enhanced surfaces, and we explore how these physical modifications influence biosensor performance metrics such as sensitivity, limit of detection, and response time. Additionally, we examine how the thickness of the enzyme layer, applied using a robotic microcontact stamping technique, affects performance, revealing a trade-off between sensitivity and response time. Our findings are further supported by a numerical model, simulated through COMSOL Multiphysics, which helps generalize the experimental results and provides valuable insights into the influence of physical design on biosensor functionality.

This work builds on previous electrode designs by systematically incorporating and evaluating surface nanostructuring and enzyme layer optimization to improve biosensor performance. The knowledge gained from this study provides design guidelines for the development of high-performance enzymatic biosensors with tailored functionalities, demonstrating that physical design modifications can significantly enhance biosensor performance with relatively simple adjustments.

2. Results and discussion

2.1. Fabrication of biosensors with different physical designs

Fig. 1 depicts biosensors with various physical designs on Pt black-coated microelectrodes functionalized with GOx through microcontact stamping. The schematic of the fabrication process (Fig. 1 (a)) and photographic images of sensors in circular/fractal design (Fig. 1 (b)) are presented, alongside SEM images of sensors in fractal design (Fig. 1 (c)). Pt microelectrodes, fabricated using conventional photolithography,

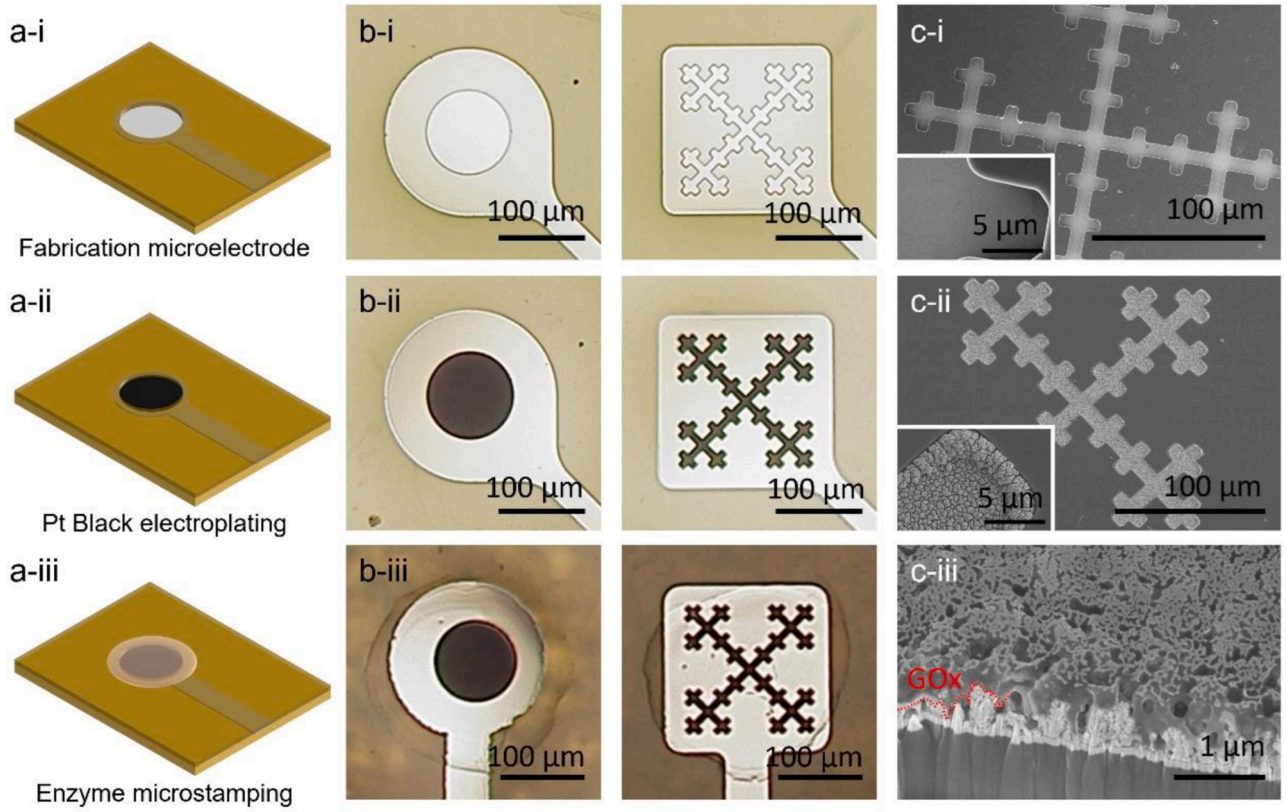

Fig. 1. Fabrication of the glucose biosensors based on microfabricated microelectrodes and enzyme microstamping. a) Schematics of the biosensor fabrication process. i) Platinum (Pt) microelectrodes are microfabricated on polyimide (PI) substrate, then insulated and defined via patterned SU-8 layer; ii) Nanostructured Pt black layer is deposited on Pt microelectrodes via electroplating; iii) Functionalization via glucose oxidase (GOx) microstamping. b) Photographic images of circular i) Pt microelectrodes, ii) Pt microelectrodes with Pt black layer, and iii) final biosensor with GOx layer. c) Scanning electron microscopy (SEM) images of fractal i) Pt microelectrodes, ii) with Pt black, iii) with GOx layer (cross-sectional view). We have labeled the GOx layer and part of the interface between it and the Pt black layer with a red dotted line.

were sandwiched between polyimide (PI) and photoresist SU-8 layers (Fig. 1 (a-i)). Circular microelectrodes had a designed diameter of 100 μm, translating to a surface area of approximately 7900 μm^2. Actual measurements from images (Fig. 1 (b-i)) showed a perimeter of 329.71 ± 5.96 μm and a surface area of 7533.79 ± 60.37 μm^2. Fractal microelectrodes images (Fig. 1 (c-i)), with the same surface area but a larger perimeter (2000 μm), exhibited a 540 % increase in perimeter-to-area ratio. Measured perimeter and surface area were 1828.36 ± 57.33 μm and 6546.77 ± 615.27 μm^2, respectively, reflecting a 538.14 % increase in perimeter-to-area ratio compared to circular microelectrodes. While both the circular and fractal geometries were designed to have the same theoretical area, differences in measured surface areas occurred due to microfabrication resolution limits, SEM and optical imaging uncertainties.

To assess surface effects, Pt black layers were added via electroplating to some microelectrodes (Fig. 1 (a-ii)). Energy-dispersive X-ray spectroscopy (EDS) showed identical compositions between Pt and Pt black surfaces (see Fig. A.1 in appendix). Photographic and SEM images confirmed retained geometries, with Pt black layers enhancing surface nanostructure. SEM magnification highlighted thicker Pt black edges (Fig. 1 (c-ii)), particularly noticeable in fractal electrodes due to their higher perimeter-to-area ratio [49].

GOx was immobilized onto microelectrodes via microcontact stamping (see Fig. A.2 in appendix). Initially, a PDMS stamp was soaked in a solution containing GOx, bovine serum albumin (BSA), and glutaraldehyde. Positioned above the microelectrode using a 3-axis motorized stage (Fig. A.2 (a)), the stamp was then lowered to deposit the GOx hydrogel solution (Fig. A.2 (b)). The stamp was re-soaked for the next microelectrode. This automated process ensured precise and swift GOx stamping (Fig. 1 (b-iii)) with minimal excess beyond the electrode openings. FIB-SEM images (Fig. 1 (c-iii)) revealed GOx/BSA/glutaraldehyde hydrogel thicknesses of 144 ± 18 nm for one stamp and 746 ± 82 nm for five stamps. Thickness linearly correlated with stamp layers, showcasing tunability. Though SEM conditions might alter the hydrogel, conventional SEM has been used previously by other researchers to image similar enzyme/BSA/glutaraldehyde hydrogels [52, 53], while cryo-SEM offers potential advantages for future enzyme hydrogel characterization [54].

2.2. Impact of microelectrode physical design on electrochemical properties

2.2.1. Electrochemical characterization

To examine physical design's impact on electrochemical properties, we considered microelectrodes with circular or fractal designs, and Pt or Pt black finish, as shown in Fig. 1 (b-ii). These sensors underwent cyclic voltammetry (CV) and electrochemical impedance spectroscopy (EIS) in blank 1X phosphate-buffered saline (PBS, pH 7.4) to assess the intrinsic electrochemical properties of the electrodes, without interference from analytes or catalytic reactions as shown in Fig. 2. Cyclic voltammograms of Pt (Fig. 2 (a)) and Pt black (Fig. 2 (b)) microelectrodes resembled prior findings [49]; compared to circular Pt, fractal Pt black had significantly higher current density at cathodic potentials, indicating enhanced electrochemical activity. Specifically, the current densities for electrode functionalization with Pt black electrodes were estimated using the electrochemical area, determined through FIB-SEM techniques. We assessed the electrochemical areas as 7578.7 μm^2 and 8580.9 μm^2 for circular and fractal platinum black electrodes respectively. Charge storage capacities (CSC) of microelectrodes were calculated from voltammograms using:

$$CSC = \frac{1}{\nu A}\int_{E_c}^{E_a} |i| dE \qquad \text{(Eq.(1))}$$

where ν is the scan rate, A is the electrode surface area, E is the potential v. Ag/AgCl (3 M NaCl) reference electrode, E_a and E_c are the CV potential endpoints, and i is the measured current. CSC is a measure of the

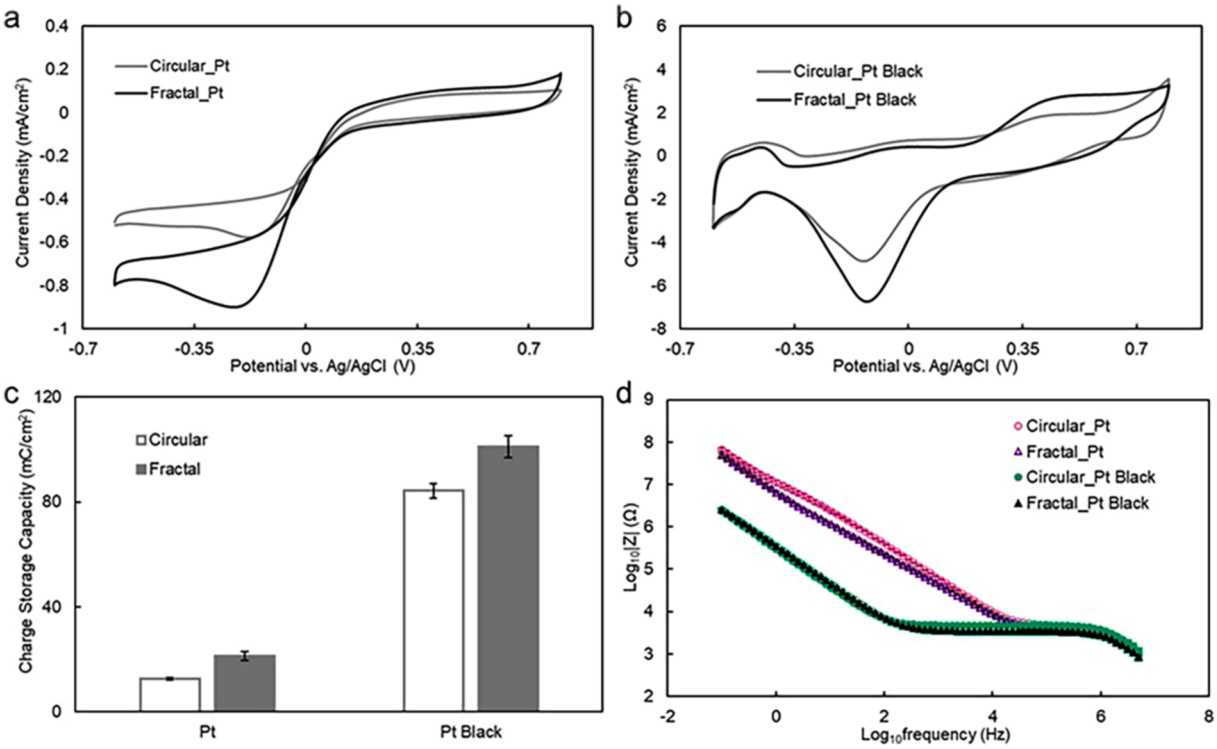

Fig. 2. Electrochemical characterization of different microelectrodes. Representative cyclic voltammogram (CV) of circular and fractal microelectrode with a) Pt and b) Pt black surfaces in 1X PBS (pH 7.4) at a scan rate of 50mV/s. c) Charge storage capacity of different microelectrodes. d) Representative impedance spectra of different microelectrodes.

ratio of an electrode's electrochemical surface area to its geometric surface area [55]. Fig. 2 (c) shows both fractal geometry and Pt black increased CSC, with Pt black showing a more pronounced effect. A two-way ANOVA revealed a significant interaction between geometry (circular v. fractal) and surface finish (Pt v. Pt black) on CSC ($F(1,12) = 9.783$, $p = 0.009$). Simple main effects analysis showed that geometry and surface finish on their own each had a statistically significant effect on CSC ($p = 6 \times 10^{-7}$ and $p = 6 \times 10^{-16}$, respectively). Both the fractal geometry and a Pt black surface finish increased CSC without having to increase the geometric surface area, which would otherwise be necessary. In other words, these results demonstrate that both fractal geometry and Pt black increased the electrode's electrochemical surface area. This agrees with our previous work. [49]

Impedance spectra from EIS (Fig. 2 (d)) indicates Pt black microelectrodes had lower impedance at low frequencies (0.1 Hz to 0.2 MHz). Fractal Pt microelectrodes exhibited the lowest impedance across all frequencies (0.1 Hz to 5 MHz), but fractal Pt black electrodes only showed lower impedance at high frequencies (200 Hz to 5 MHz). Results align with expectations for nanostructured surface finish and geometric area, enlarging the electrochemical surface area and lowering impedance below cutoff frequency. High-frequency impedance, determined by access resistance, scales with geometric surface area [56]. CV and EIS suggest fractal geometry and Pt black surface boost electrochemical activity with the same geometric area. More Pt black deposition at the perimeter may explain the superior electrochemical activity of fractal Pt black electrodes [57,58] (inset of Fig. 1 (c-ii)). Future work will vary Pt black amount and size to explore further.

Next, we explored microelectrode behaviors and charge storage capacities of the biosensor with a single GOx enzyme layer. In Fig. 3, we show the results with different geometries (fractal and circular) and surface finishes (Pt and Pt Black) at varying H_2O_2 concentrations (0, 0.1mM, and 0.2mM). Comparing CVs of Pt surface finish (Fig. 3 (a) and (c)) with Pt Black surface finish (Fig. 3 (b) and (d)), we observe higher electrochemical activity with Pt Black. Fractal geometries show greater reactivity, especially at higher concentrations.

Fig. 3 (e) bar graph confirms trends in voltammograms, showing superior charge storage capacity of fractal geometries across all concentrations and finishes. Pt Black notably outperforms Pt, especially at higher concentrations.

Similarly, we characterized the biosensor with a single GOx enzyme layer for different glucose concentrations. Fig. 4 presents CVs for fractal and circular geometries coated with either Pt or Pt Black, with glucose concentrations at 0 and 1mM. These plots highlight sensitivity to surface morphology and composition, with Pt Black surfaces exhibiting higher current densities, particularly for fractal geometry. Fig. 4 (e) bar chart demonstrates a significant increase in charge storage capacity for fractal

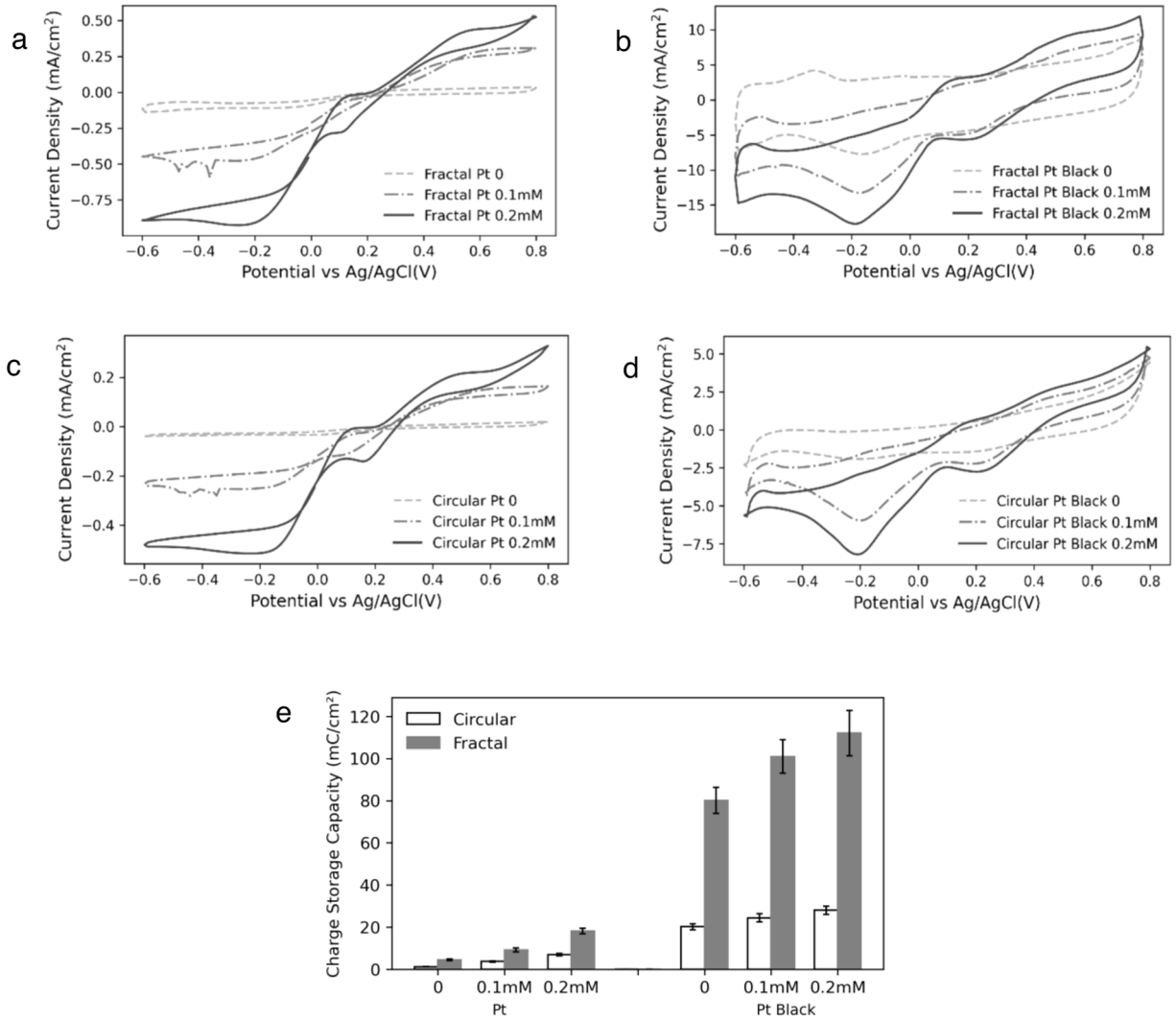

Fig. 3. Electrochemical characterization representing CVs for (a) fractal Pt, (b) fractal Pt Black, (c) circular Pt, and (d) circular Pt Black microelectrodes in 1X PBS (pH 7.4) at a scan rate of 50mV/s with hydrogen peroxide (H_2O_2) at 0, 0.1mM, and 0.2mM in the presence of a single GOx layer. (e) The charge storage capacities of different microelectrodes.

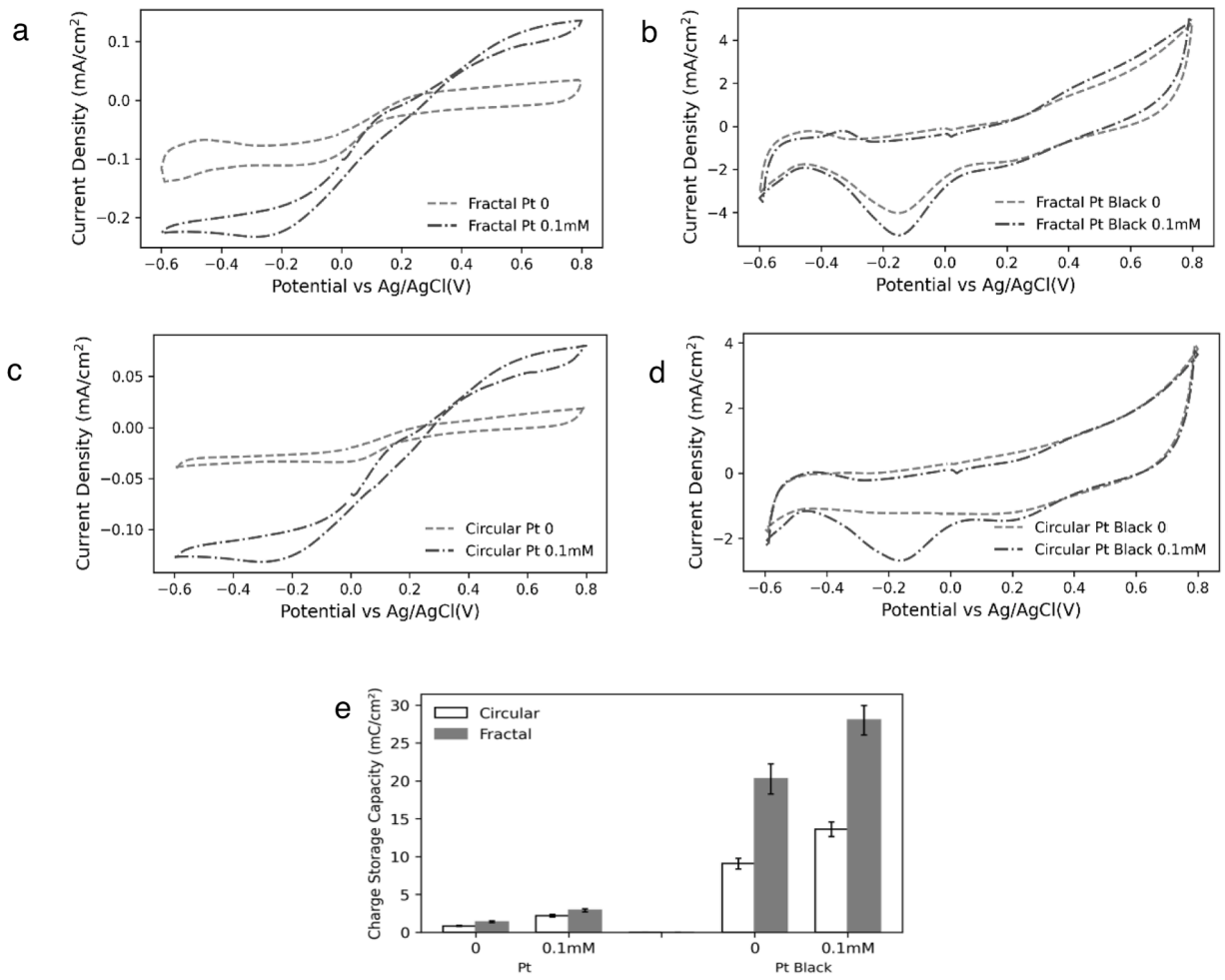

Fig. 4. Electrochemical characterization representing CVs for (a) fractal Pt, (b) fractal Pt Black, (c) circular Pt, and (d) circular Pt Black microelectrodes in 1X PBS (pH 7.4) at a scan rate of 50mV/s with glucose at 0 and 1mM in the presence of a single GOx layer. (e) The charge storage capacities of different microelectrodes.

electrodes compared to circular ones when coated with Pt Black instead of Pt alone. CVs with five GOx layers are also conducted; results in Fig. A.3 and Fig. A.4 in appendix show the impact on current density and charge storage capacity. Overall, trends indicate decreased current density and lower charge storage capacity with multiple GOx layers, as discussed further in Section 2.4.

In the cyclic voltammograms of Figs. 3 and 4, prominent anodic peaks are observed around +0.4 V to +0.6 V, corresponding to the oxidation of hydrogen peroxide (H_2O_2) at the platinum surface. In fractal Pt black microelectrodes, this peak is sharper and of higher intensity compared to circular Pt electrodes, indicating enhanced catalytic activity due to the increased surface roughness and perimeter-to-area ratio of the fractal geometry. This improvement is further supported by the higher current densities observed at lower potentials. The fractal geometry offers a significantly larger perimeter-to-area ratio compared to the circular design, resulting in a higher number of active sites for electrochemical reactions. This leads to increased current densities and greater sensitivity, as observed in the cyclic voltammetry results. The enhanced mass transport and electron transfer kinetics associated with fractal electrodes contribute to the sharper and more pronounced redox peaks, particularly at higher analyte concentrations. Pt black deposition substantially increases the electrochemical surface area by introducing nanostructuring, which enhances electron transfer kinetics and reduces impedance. This is reflected in the higher current densities and shifted redox peaks observed in Pt black-coated electrodes compared to their smooth Pt counterparts. In particular, the Pt black surface facilitates the oxidation and reduction of H_2O_2 and glucose more efficiently, resulting in sharper peaks at both anodic and cathodic potentials. Hysteresis between the forward and reverse scans is more pronounced in fractal electrodes compared to circular electrodes, likely due to capacitive charging effects associated with the larger electrochemical surface area. The increased number of active sites in fractal electrodes allows for greater charge accumulation, resulting in the observed hysteresis, particularly at higher scan rates.

2.2.2. *Amperometric response to H_2O_2*

First-gen enzymatic biosensors utilize enzymes like glucose oxidase (GOx) to convert glucose into H_2O_2, acting as a mediator to the transducer (e.g., Pt electrode). Literature suggests H_2O_2 oxidation potential at Pt ranges around +0.2 to +0.3 V vs. Ag/AgCl, linked to Pt oxidation [55, 59]. H_2O_2 oxidation relies on Pt oxidation to $Pt(OH)_2$, forming Pt $(OH)_2{\cdot}H_2O_2$ complex [60]. CV results (Figs. 3 and 4) support Pt electrode oxidation at anodic potentials, particularly noticeable with Pt Black electrodes, leading to selecting +0.5 V vs. Ag/AgCl (3 M NaCl) for amperometric measurements of H_2O_2 and glucose.

Efficient H_2O_2 transport and catalysis at the transducer are crucial for biosensor performance. Based on design shown Fig. 1 (b-iii) – with enzyme deposition- we assessed the electrocatalytic properties of microelectrodes with different designs regarding amperometric response to sequential H_2O_2 additions at +0.5 V vs. Ag/AgCl (3 M NaCl) (Fig. 5). For CSC, a two-way ANOVA analyzed the impact of geometry (circular vs. fractal) and surface finish (Pt vs. Pt black) on H_2O_2 sensitivity. There was a significant interaction between geometry and surface finish ($F(1,8) = 50.462$, $p = 0.0001$). Both geometry and surface finish individually had

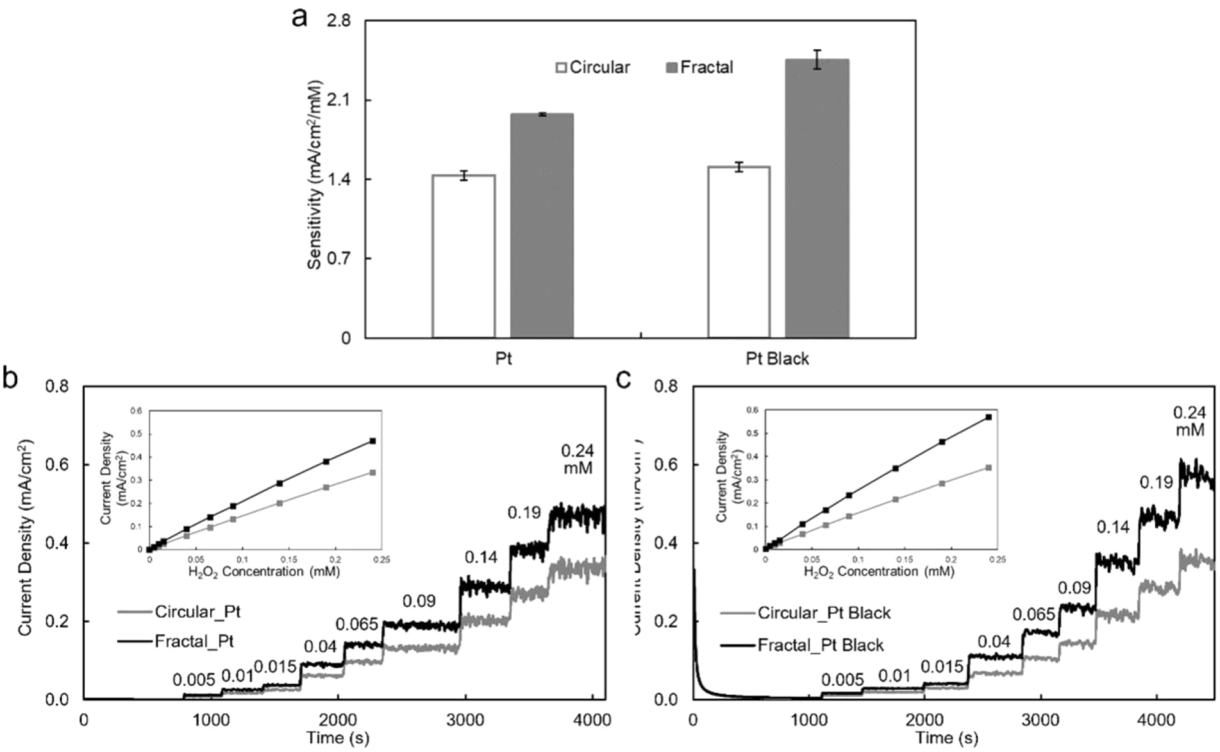

Fig. 5. Electrocatalytic response of different microelectrodes to H_2O_2. a) Summary of H_2O_2 sensitivity of different microelectrodes. Representative amperometric response of circular and fractal microelectrode with b) Pt and c) Pt black surfaces. Insets in b) and c) show the corresponding current response with regard to various H_2O_2 concentrations.

statistically significant effects ($p = 5 \times 10^{-9}$ and $p = 9 \times 10^{-6}$, respectively).

Fig. 5 (a) and Table 1 summarize an important interaction between microelectrode geometry and surface nanostructuring affecting H_2O_2 sensitivity. Fractal Pt microelectrodes did not show significantly higher sensitivity compared to circular Pt ones. However, Pt black microelectrodes of both geometries were notably more sensitive than their Pt counterparts. Intriguingly, fractal geometry amplified the sensitivity enhancement by Pt black. This could be attributed to increased Pt black deposition around the electrode perimeter (Fig. 1 (a)), along with mass transfer constraints for H_2O_2 oxidation on circular Pt black electrodes. The role of diffusional geometry on sensitivity is elucidated in the numerical modeling section in the appendix.

Alongside sensitivity, we analyzed linearity and the limit of detection (LOD) of the microelectrode. In Fig. 5 (b) and (c) insets, covering the 0–0.24 mM H_2O_2 range, all four physical design combinations demonstrated outstanding linearity, with R^2 values surpassing 0.998. The LOD was calculated using the following equation:

$$LOD = \frac{3\sigma}{S} \quad \text{(Eq.(2))}$$

where σ is the standard deviation of the baseline noise (zero analyte concentration), and S is sensitivity. Notably, fractal geometry consistently decreased the LOD of H_2O_2, regardless of surface nanostructuring (refer to Table 1). Despite Pt black improving sensitivity to H_2O_2 and reducing impedance (Fig. 2 (d)), Pt black microelectrodes exhibited higher LODs compared to Pt. This is attributed to increased baseline noise during H_2O_2 calibration, influenced by factors such as magnetic stirring and nonfaradaic interactions with the electrode and PBS [61]. The nonfaradaic interaction noise correlates with electrode surface area, with Pt black microelectrodes having significantly larger electrochemical surface areas than bare Pt microelectrodes.

Table 1
Summary of response of microelectrodes with different physical design to H_2O_2.

		Sensitivity (in μA·mM^{-1}·cm^{-2})	Linearity (R^2)	LOD (in μM)
Circular	Pt	1430 ± 40	1.000	0.2
	Pt Black	1510 ± 40	0.998	1
Fractal	Pt	1970 ± 10	0.999	0.1
	Pt Black	2460 ± 80	0.999	0.5

2.3. Impact of physical design on biosensor performance

2.3.1. Impact on biosensor sensitivity

We tested GOx immobilization on microelectrodes in various designs via microcontact stamping, examining the impact of circular/fractal geometry and Pt/Pt black surface finish on biosensor performance. Traditional enzyme immobilization involves drop-casting using a microsyringe, which is labor-intensive and low-throughput [62]. Other methods like robotic dispensing [63] and PDMS microstamping [64] offer alternatives. We innovatively employed a robotic PDMS microcontact stamping method, blending automation with spatial precision for optimal results.

Fig. 6 and Table 2 present calibration results for microelectrode biosensors spanning 0–10 mM glucose. Glucose biosensor sensitivities based on physical design are compared in Fig. 6 (a), with representative current vs. time traces and glucose calibration curves in Fig. 6(b) and (c). Each physical design exhibited stepwise responses to glucose boluses, indicating robust sensing capabilities. We evaluated six biosensor shank arrays, each containing 5 to 8 individual working microelectrode biosensors, with half featuring Pt surfaces and the rest Pt black. A three-way ANOVA, considering geometry (circular vs. fractal) and surface finish (Pt vs. Pt black) with device nested within geometry, revealed a significant interaction between geometry and surface finish ($F(1,28) = 16.713$, $p = 0.0003$). Device nested within geometry also exhibited a

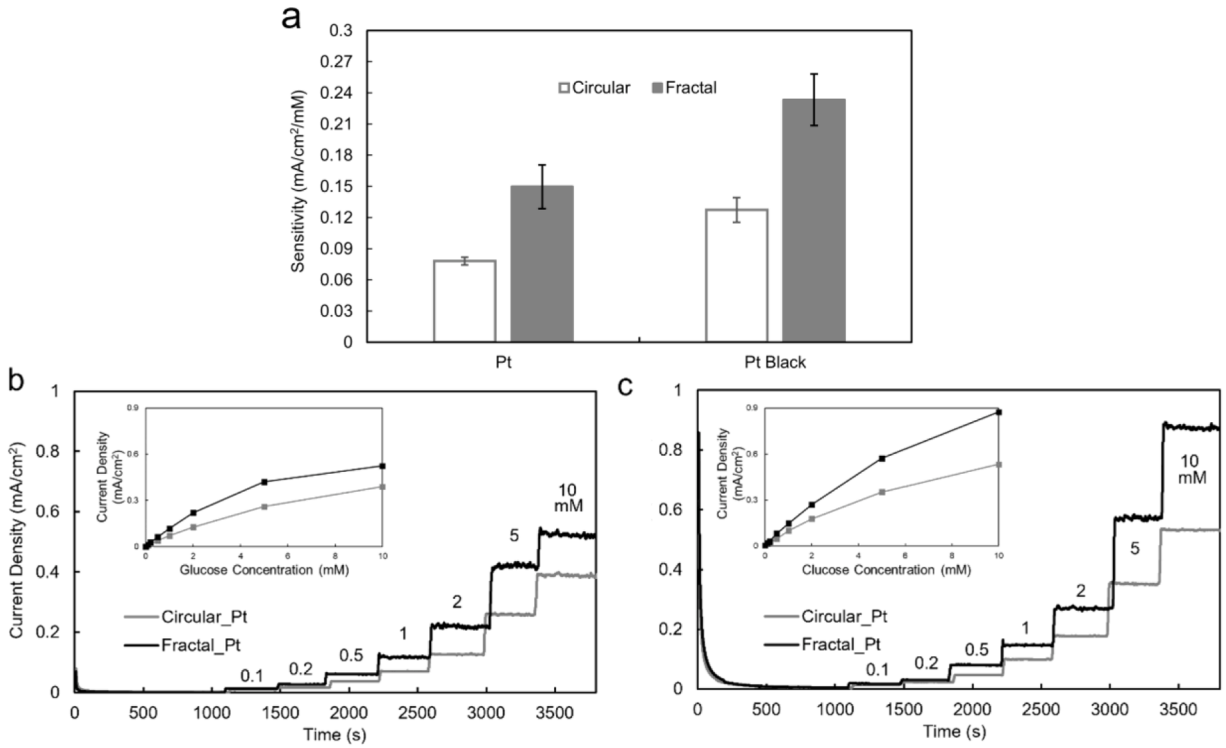

Fig. 6. Response of biosensors made of different microelectrodes to glucose. a) Summary of glucose sensitivity of biosensors made of different microelectrodes. Representative amperometric response of biosensors made of circular and fractal microelectrode with b) Pt and c) Pt black surfaces. Insets in b) and c) show the corresponding current response regarding various glucose concentrations.

Table 2
Summary of response of biosensors with different physical design to glucose.

		Sensitivity (in μA·mM^{-1}·cm^{-2})	Linearity (R^2)		LOD (in μM)
			0–5mM	0–10mM	
Circular	Pt	78.1 ± 3.6	0.991	0.971	3.0
	Pt Black	127.3 ± 11.9	0.988	0.971	9.5
Fractal	Pt	149.7 ± 21.1	0.984	0.915	1.0
	Pt Black	233.3 ± 24.9	0.994	0.976	6.7

significant effect ($p = 0.007$), albeit less pronounced than geometry ($p = 5 \times 10^{-6}$) and surface finish ($p = 2 \times 10^{-15}$), either individually or their interaction.

The results shown in Figs. 5 and 6 reveal that fractal microelectrodes combined with Pt black enhance sensitivity to both glucose and H_2O_2. However, Pt black alone significantly improved circular microelectrode sensitivity to glucose, unlike with H_2O_2. The larger size, lower diffusivity, and slower enzyme kinetics of glucose likely account for this difference compared to Pt- H_2O_2 oxidation kinetics. The geometry of residual GOx extending beyond circular and fractal electrodes may have also contributed, as faint halos are visible in Fig. 1 (b-iii). The GOx layers around both electrode types are similar in shape and size, leading to comparable H_2O_2 production and similar GOx layer-to-surface area ratios. Fractal electrodes feature interfaces between residual GOx and electrode perimeters where Pt deposition is enhanced. Future research could disentangle the impact of residual GOx using finer PDMS stamps or alternative immobilization techniques, like electropolymerization.

We estimated performance metrics, including sensitivity in the linear region, by calibrating the experimental response using the Michaelis-Menten equation. Aside from sensitivity, the limit of detection (LOD) and linearity of glucose biosensors were evaluated. For Pt-finished microelectrodes, circular and fractal biosensors exhibited LODs of 3 μM and 1 μM, respectively, while Pt black microelectrodes showed LODs of 9.5 μM and 6.7 μM. Changing from circular to fractal design reduced the LOD but switching from Pt to Pt black increased it due to higher baseline noise. All biosensor types maintained good linearity ($R^2 \geq 0.984$) between 0–5 mM glucose concentration (see Fig. A.5(a) in appendix). Beyond this range, up to 10 mM, linearity decreased but R^2 remained ≥ 0.915, indicating some response saturation.

The reusability and stability of the glucose biosensors were assessed by monitoring sensitivity changes during storage in 1X PBS at 4°C (see Fig. A.5(b) in appendix). After three weeks, the biosensors experienced a 46.3 % sensitivity loss but remained functional. This loss is likely due to enzyme degradation or reduced activity. Future work will explore surface finish changes over time using optical and electrochemical methods and will compare the stability of fractal Pt black-based biosensors with bare-Pt and circular biosensors. Overall, these findings highlight that microcontact stamping is an effective method for functionalizing microelectrodes for glucose biosensors.

2.4. Impact of enzyme thickness on biosensor performance

We repeatedly used the microcontact stamping process on each electrode after the enzyme hydrogel solution dried (about one minute). Each application formed a new GOx layer, increasing the enzyme hydrogel's thickness and the number of GOx enzymes near the electrodes. This should improve sensitivity by enhancing the H_2O_2 production rate from glucose. However, as the enzyme hydrogel thickens, it increases the distance for H_2O_2 diffusion, slowing mass transfer and oxidation, which reduces sensitivity and lengthens response time. Huang et al. (2020) investigated this phenomenon using linear sweep voltammetry to estimate H_2O_2 diffusivity through enzyme hydrogels on Pt electrodes.

We characterized biosensors functionalized with one layer (Figs. 3 and 4) and five enzyme layers (see Figs. A.3 and A.4 in appendix) using CV measurements. Previous observations indicated a tradeoff between

faster response time with fewer enzyme layers and greater sensitivity with more. We quantified the impact of one and five GOx layers on fractal Pt microelectrodes, evaluating sensitivity, response time, and LOD. The response times were defined as the time required for the sensor to reach 90 % of its final steady-state current (T90) after glucose addition. This was calculated by determining the steady-state current, calculating 90 % of this value, and recording the time it took for the current to reach this level after glucose addition. A potential of 0.5 V vs. Ag/AgCl (3 M NaCl) was applied, falling within the H_2O_2 mass transport control range, as shown in Figs. 2 and 3. Fig. 7 (a) and Table 3 reveal that biosensors with five GOx layers had higher sensitivity (219.1 ± 22.8 $\mu A \cdot mM^{-1} \cdot cm^{-2}$) compared to one-layer biosensors (92.4 ± 16.0 $\mu A \cdot mM^{-1} \cdot cm^{-2}$), but exhibited longer response times (9.0 ± 0.8 s vs. 6.0 ± 1.0 s). Fig. 7 (b) shows the increased response and delayed reaction of five-layer biosensors as glucose concentration rises from 1 to 2 mM.

The LOD of biosensors with one and five enzyme layers was calculated and compared. Glucose biosensors with one layer had an LOD of 1.4 μM, while those with five layers had an LOD of 0.6 μM, which contributes to their higher sensitivity. These results align with findings from other studies using the conventional drop-casting technique. This consistency reinforces robotic microcontact stamping as an effective alternative enzyme immobilization method. Future research should optimize the enzyme layer count and hydrogel formulation to achieve the desired sensitivity or response time.

2.5. Interpretation and validation of experimental response

Nair and Alam's model studies current transients in electrochemical sensors, emphasizing the importance of electrode geometry and functionalization [39–42]. They showed that modifying the heterogeneous rate constant k_0 in the Butler-Volmer equation can account for different electrode shapes and finishes, enhancing sensor performance, see Interpretation of physical design in appendix for further details. Specifically, we implemented a numerical model on COMSOL Multiphysics to self-consistently interpret the physical origin of experimentally observed amperometric responses as a function of the physical designs. Once calibrated against the experimental settings, the model predicted the impact of an arbitrary physical design on amperometric response and suggested guidelines for biosensor optimization [10,11,36–39]. Mathematical modeling and amperometric operation in appendix provide further insights. The corresponding settings of the numerical model, reported in Table A.1 of Appendix, are estimated either from experimental characterization of the sensor or from earlier studies on modeling of enzymatic and non-enzymatic biosensors for both in-vitro and in-situ measurements [10,11,65,26,66]. Given the parameters reported in appendix section, Table A.1 (unless otherwise stated), we validate the following experimental results:

Table 3
Summary of response of fractal biosensors with different enzyme thickness to glucose.

	Sensitivity (in $\mu A \cdot mM^{-1} \cdot cm^{-2}$)	LOD (in μM)	Response time (s)
1 layer	92.4 ± 16.0	1.4	6.0 ± 1.0
5 layer	219.1 ± 22.8	0.6	9.0 ± 0.8

1. A linear increase in current density step results from increased glucose concentrations (Fig. 8); An improved sensitivity results from an increased heterogeneous rate constant k_0 thanks to electrode geometry and electrode finish designs [11];
2. An improved sensitivity but slower response time results from an increased enzyme layer (Fig. 9);
3. Fig. A.7 in appendix section shows the independence of response time on glucose concentration for specific conditions; A thicker permselective membrane may potentially improve sensor selectivity while degrading sensitivity and increasing response time of the sensor [67].

First, we validated the amperometric response v. sequential addition of glucose (Fig. 8 (a)). A higher glucose concentration leads to a higher generated current. Due to limited addition of analyte at $t = 0$, the generated current increases until reaching a peak value. Then, it would decay to zero at time = infinity. However, before the system is depleted of analyte molecules, a new addition of analyte is added to the solution. By sequential addition of analyte, the amperometric response shows a staircase-like profile. Compared to experiments which assume a three-dimensional structure and constant supply of analyte from any direction, here, a one-dimensional system is simulated. Therefore, the depletion process takes place at a faster rate. Fig. 8 also shows the beneficial impact of improved heterogenous constant k_0 on amperometric response. By either increasing the perimeter-to-area ratio (planar v. fractal) or improving electrode quality for electron transfer (Pt black v. Pt), the generated peak current increases correspondingly. Therefore, biosensors functionalized with improved k_0 exhibit higher sensitivity (Fig. 8 (b)), as shown in experiments (Figs. 5 and 6).

Second, we evaluated the impact of enzyme thickness on amperometric response. Fig. 9 shows that, by increasing the enzyme thickness, the overall current peak increases and the transient response gets delayed, as shown in experiments (Fig. 7). Qualitatively, a thicker enzyme domain provides a higher number of active centers for H_2O_2 conversion, leading to a higher current. However, thicker the domain longer time is required for H_2O_2 molecules to diffuse towards the electrode surface. By accounting for the complete sequence of events (glucose diffusion, glucose conversion, peroxide diffusion, current generation), a longer time is required compared to peroxide diffusion and reaction shown in Fig. A.6 in appendix.

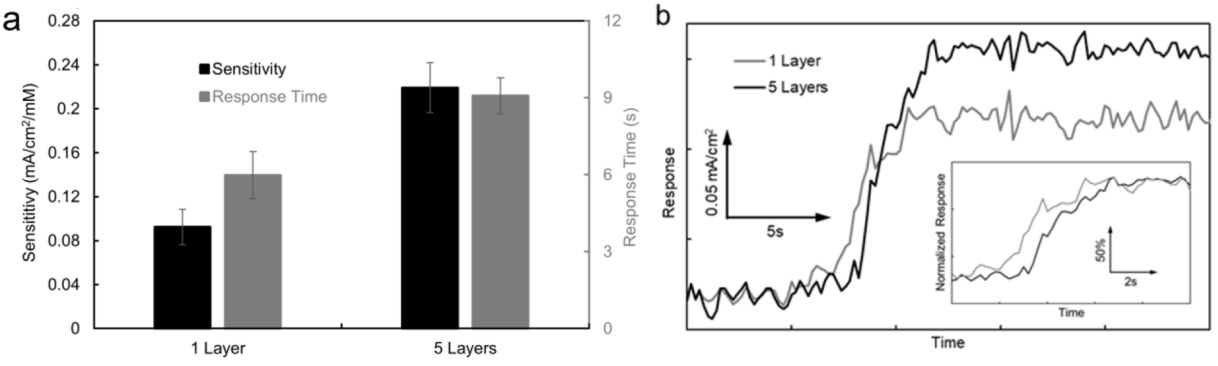

Fig. 7. Effects of the number of GOx layers on the performance of the fractal glucose biosensors. a) Sensitivity and response time of glucose biosensors made of either one or five layers of GOx. b) Representative responses to 2 mM glucose from glucose biosensors made of either one or five layers of GOx. Inset shows their normalized responses.

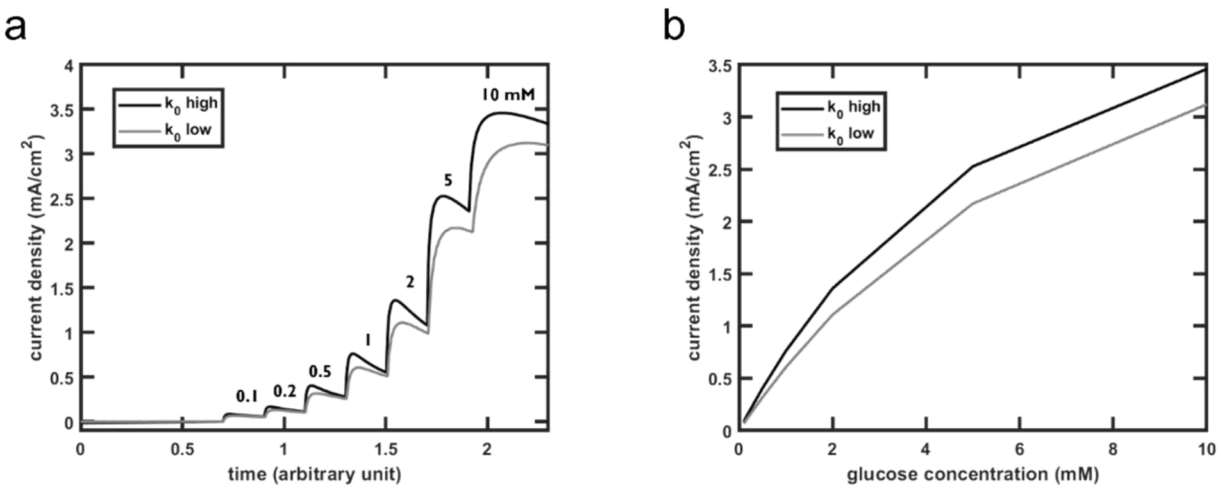

Fig. 8. COMSOL-based numerical simulations: Effect of limited addition of glucose (a) on amperometric response and sensor sensitivity (b) for an electrode system with small heterogeneous rate constant ($k_0 = 3{\cdot}10^{-7}\ m{\cdot}s^{-1}$ for circular or smooth Pt electrode geometry) v. high heterogeneous rate constant ($k_0 = 3{\cdot}10^{-5}\ m{\cdot}s^{-1}$ for fractal or Pt black electrode geometry [11]). Here, we assume a difference of two orders of magnitude to qualitatively show the impact of a low k_0 on the performance, considering the enhanced performance of high k_0 typical of nanostructured and non-planar geometries [10,11,18,65].

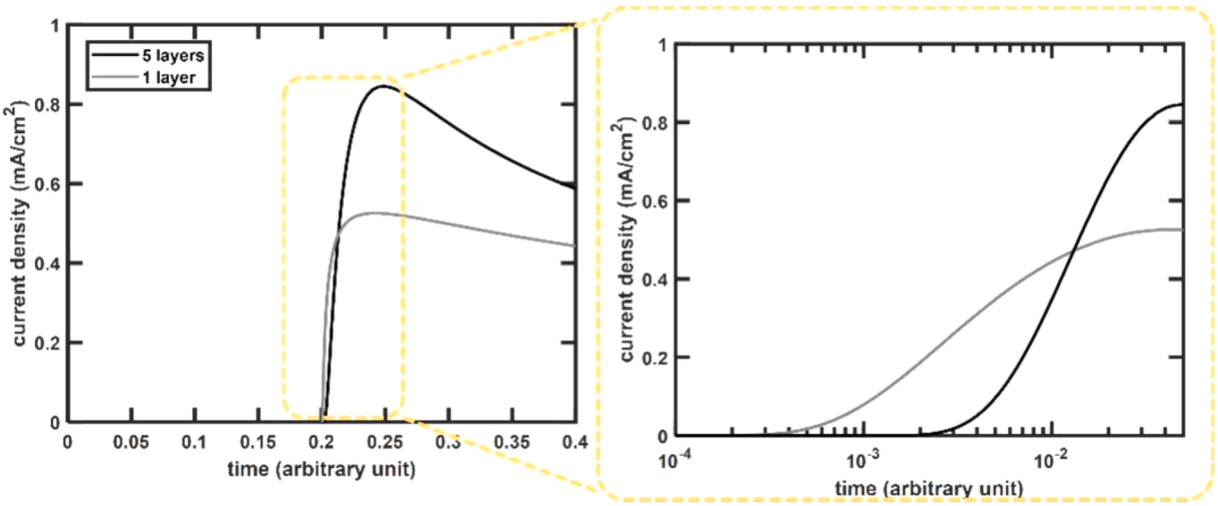

Fig. 9. COMSOL-based numerical simulations: Effect of enzyme thickness on amperometric response. Onset displays the slower response associated with a thicker enzyme domain.

3. Methods

3.1. Fabrication of microelectrodes

We used photolithography to fabricate platinum microelectrodes between a polyimide substrate and a patterned SU8 insulation layer. Some Pt microelectrodes were electroplated with Pt black in 17.5 mM hexachloroplatinic acid 0.03 M acetate buffer (pH 5.6), applying 0 V v. Ag/AgCl (3 M NaCl) (BASi, West Lafayette, IN) until accumulated charge reached 0.02 μC/μm^2. This charge density is based on the geometric (2D planar) area and not the changing electrochemical surface area. We determined 0.02 μC/μm^2 by first measuring the geometric surface area from an optical image with a digital microscope (Hirox USA Inc., Hackensack, NJ, USA). Then, we multiplied 0.02 μC/μm^2 by that area to get a charge. Finally, in the potentiostat's software (EC-Lab), we set a charge limit for amperometry, so the potentiostat would stop deposition once that charge was reached. The potentiostat was a SP-200 (Bio-Logic.Inc, Seyssinet-Pariset, France), and a Pt wire (BASi, West Lafayette, IN) was used as counter electrode. Controlling charge density based on geometric surface area instead of time means the deposition time will vary somewhat from electrode to electrode. However, this method of control reduces variation in sensitivity since net charge corresponds to film growth [68,69].

3.2. Morphological characterization

We photographed microelectrodes using a Hirox digital microscope. SEM and EDS images came from a Hitachi S-4800 Field Emission SEM (Schaumburg, IL) with Oxford X-Max^N 80 (Concord, MA). For SEM, accelerating voltage was 5 kV. For EDS, accelerating voltage was 10 kV; emission current was 15 μA, and X-ray signals were collected for 120 s. Prior to SEM/EDS, a thin layer of Au-Pd was sputtered onto samples using a desktop coater (SPI Sputter, West Chester, PA). Cross sectioning microelectrodes with enzyme layers was done using Helios G4 Dual Beam FIB (Thermo Scientific, Waltham, MA).

3.3. Enzyme immobilization

We stamped enzyme solution onto microelectrodes. We molded PDMS (SYLGARD® 184, Sigma Aldrich, St. Louis, MO, cat. 761036)

stamps by pouring them into 10 μL pipette tips and baking for 2 h at 70°C. Then, we removed the PDMS stamps with tweezers and mounted them onto 25-gauge precision stainless steel dispense tips (Nordson EFD, East Providence, RI). Once we mounted the PDMS stamps, we screwed the precision dispense tips onto a syringe barrel fastened into a 3-axis motorized stage equipped with cameras (Pro EV3, Nordson EFD, East Providence, RI). This allowed us to manipulate the PDMS stamp according to a pre-defined program made in the Nordson EFD software. Basically, we placed a <1 mL reservoir of enzyme hydrogel solution off but near the electrode array and programed the robot to dip the stamp in the enzyme hydrogel drop each time before stamping an electrode. We stamped electrodes serially, and we waited at least one minute before re-stamping the same electrode. Therefore, each layer had time to adequately dry. Enzyme hydrogel solution consisted of 0.1 % glutaraldehyde (grade II, 25 % in H_2O, Sigma Aldrich, St. Louis, MO), 0.8 % bovine serum albumin (BSA, Sigma Aldrich, St. Louis, MO, cat. A3059), and 0.2 U/μL glucose oxidase (MP Biomedicals LLC, Solon, OH). After depositing the enzyme hydrogel solution by stamping, we left the biosensors in dark, dry room-temperature place for at least 2 days, so glutaraldehyde could sufficiently complete crosslinking.

3.4. Electrochemical characterization

CV and EIS results were collected using potentiostat SP-200 (Bio-Logic Inc, Seyssinet-Pariset, France). During CV, potential was swept between –0.6V and 0.8V v. Ag/AgCl (3 M NaCl) at 50 mV/s. During EIS, the perturbation potential was sinusoidal with 30 mV amplitude and 0.1 Hz to 5 MHz frequency range. H_2O_2 (Thermo Scientific, Waltham, Massachusetts) and glucose (Sigma-Aldrich, St. Louis, MO) calibration was performed at 0.5 V v. Ag/AgCl (3 M NaCl) in 1X phosphate-buffered saline (PBS, pH 7.4, Invitrogen, Carlsbad, CA) stirred throughout the entirety of all calibrations by a magnetic bar at 250 rpm. A graphite rod (Eisco Labs, Victor, NY) was used as counter electrode. For Figs. 3 and 4, we filtered H_2O_2 and glucose calibration amperometric data with a 10^{-s} moving average filter to reduce noise from stirring. Small-volume boluses (2–200 μL) of concentrated H_2O_2 or glucose were added near the edge of a 100-mL beaker initially containing 20 mL 1X PBS. Meanwhile, the biosensors were placed near the center of the beaker, so the distance from analyte addition to biosensor working electrode was approximately 25 mm.

4. Conclusion

When it comes to improving biosensor performance, modifying physical design over material and biological design has numerous advantages. These include low additional material cost, short design cycle times, no new concerns for biocompatibility, and minimal investment in additional tooling. In this work, we focused on the physical design aspects of the biosensors and studied how they affected the sensor performance such as sensitivity, response time, linearity, and LOD. The results, supported by a consistent numerical model and theoretical framework, suggest using fractal electrodes significantly increases sensitivity to H_2O_2 and glucose, compared to circular electrodes. This design change can be easily incorporated into conventional MEMS fabrication processes with practically no increase in cost. Nanostructuring the electrode surface by Pt black deposition and increasing enzyme matrix thickness similarly increased sensitivity and mean only a small relative increase in cost. Moreover, robotic microcontact stamping proved to be a useful method for automated, precise, and tunable immobilization of GOx. This technique can be further improved by molding stamps into custom shapes matching target electrodes, for example, the fractal microelectrode shapes presented here. Future work should extend investigation of fractal microelectrodes with or without surface nanostructuring for other electrochemical measurement techniques, biorecognition elements, and target analytes, e.g. electrochemical impedance spectroscopy, aptamers, and neurotransmitters, respectively.

CRediT authorship contribution statement

Jian Xu: Writing – original draft, Visualization, Validation, Methodology, Investigation, Conceptualization. **Marco Fratus:** Writing – review & editing, Writing – original draft, Validation, Software, Methodology, Conceptualization. **Ankit Shah:** Writing – review & editing, Visualization, Validation, Software, Resources, Data curation, Conceptualization. **James K. Nolan:** Writing – original draft, Visualization, Validation, Methodology, Data curation, Conceptualization. **Jongcheon Lim:** Software, Conceptualization. **Chi Hwan Lee:** Supervision. **Muhammad A. Alam:** Supervision. **Hyowon Lee:** Writing – review & editing, Supervision, Resources, Methodology, Funding acquisition, Conceptualization.

Declaration of competing interest

The authors declare the following financial interests/personal relationships which may be considered as potential competing interests: Hyowon Lee reports financial support was provided by National Science Foundation, Eli Lilly. If there are other authors, they declare that they have no known competing financial interests or personal relationships that could have appeared to influence the work reported in this paper.

Acknowledgments

This work was supported in part by the National Science Foundation (United States) under the grant ECCS-1944480 and Eli Lilly Connected Care Program.

The authors gratefully thank Michelle Pearson for coordinating the operations between PIs groups and Eli Lilly and Company.

Supplementary materials

Supplementary material associated with this article can be found, in the online version, at doi:10.1016/j.electacta.2024.145270.

Data availability

Data will be made available on request.

References

[1] X. Qi, S. Wang, T. Li, X. Wang, Y. Jiang, Y. Zhou, X. Zhou, X. Huang, P. Liang, Biosens. Bioelectron. 173 (2021) 112822.
[2] L. Chao, Y. Liang, X. Hu, H. Shi, T. Xia, H. Zhang, H. Xia, J. Phys. D. Appl. Phys. 55 (2021) 153001.
[3] Z. Kotsiri, J. Vidic, A. Vantarakis, J. Environ. Sci. 111 (2022) 367–379.
[4] Y. Lu, Q. Yang, J. Wu, TrAC. Trend. Analyt. Chem. 128 (2020) 115914.
[5] I. Lee, D. Probst, D. Klonoff, K. Sode, Biosens. Bioelectron. 181 (2021) 113054.
[6] S. Bian, B. Zhu, G. Rong, M. Sawan, J. Pharm. Anal. 11 (2021) 1–14.
[7] P. Li, G.H. Lee, S.Y. Kim, S.Y. Kwon, H.R. Kim, S. Park, ACS Nano 15 (2021) 1960–2004.
[8] S. Mondal, N. Zehra, A. Choudhury, P.K. Iyer, ACS Appl. Bio. Mater. 4 (2021) 47–70.
[9] M.A. Alam, A. Saha, M. Fratus, Innov. Emerg. Technolog. 09 (2022).
[10] X. Jin, A.J. Bandodkar, M. Fratus, R. Asadpour, J.A. Rogers, M.A. Alam, Biosens. Bioelectron. 168 (2020) 112493.
[11] M. Fratus, M.A. Alam, Appl. Phys. Lett. 122 (2023) 054102.
[12] G. Yang, Z. Xiao, C. Tang, Y. Deng, H. Huang, Z. He, Biosens. Bioelectron. 141 (2019) 111416.
[13] M. Ouyang, D. Tu, L. Tong, M. Sarwar, A. Bhimaraj, C. Li, G.L. Coté, D. Di Carlo, Biosens. Bioelectron. 171 (2021) 112621.
[14] B.D. La Franier, M. Thompson, Biosens. Bioelectron. 135 (2019) 71–81.
[15] T.N.H. Nguyen, J.K. Nolan, H. Park, S. Lam, M. Fattah, J.C. Page, H.-E. Joe, M.B. G. Jun, H. Lee, S.J. Kim, R. Shi, H. Lee, Biosens. Bioelectron. 131 (2019) 257–266.
[16] Y. Sun, T.N.H. Nguyen, A. Anderson, X. Cheng, T.E. Gage, J. Lim, Z. Zhang, H. Zhou, F. Rodolakis, Z. Zhang, I. Arslan, S. Ramanathan, H. Lee, A.A. Chubykin, ACS Appl. Mater. Interface. 12 (2020) 24564–24574.

[17] M.S. Khan, S.K. Misra, A.S. Schwartz-Duval, E. Daza, F. Ostadhossein, M. Bowman, A. Jain, G. Taylor, D. McDonagh, L.T. Labriola, D. Pan, ACS Appl. Mater. Interface. 9 (2017) 8609–8622.
[18] M. Fratus, J. Lim, J. Nolan, E. Madsen, Y. Dai, C.H. Lee, J.C. Linnes, H. Lee, M. A. Alam, IEEE. Sens. J. 23 (2023) 14285–14294.
[19] N. Wongkaew, M. Simsek, C. Griesche, A.J. Baeumner, Chem. Rev. 119 (2019) 120–194.
[20] A. Khanmohammadi, A. Aghaie, E. Vahedi, A. Qazvini, M. Ghanei, A. Afkhami, A. Hajian and H. Bagheri, *Talanta.*, DOI:10.1016/J.TALANTA.2019.120251.
[21] J. Zhang, J. Xu, J. Lim, J.K. Nolan, H. Lee, C.H. Lee, Adv. Healthc. Mater. 10 (2021) 2100194.
[22] B. Zhu, X. Li, L. Zhou, B. Su, Electroanalysis. 34 (2022) 237–245.
[23] I.S. Kucherenko, O.O. Soldatkin, D.Y. Kucherenko, O.V. Soldatkina, S. V. Dzyadevych, Nanoscale Adv. 1 (2019) 4560–4577.
[24] Z. Zhu, L. Garcia-Gancedo, A.J. Flewitt, H. Xie, F. Moussy, W.I. Milne, mdpi.com 12 (1991) 5996–6022.
[25] M.M. Rahman, A.J.S. Ahammad, J.H. Jin, S.J. Ahn, J.J. Lee, Sensors 10 (2010) 4855–4886.
[26] M. Fratus, M.A. Alam, Biosens. Bioelectron. 255 (2024) 116238.
[27] V. Buk, M.E. Pemble, Electrochim. Acta. 298 (2019) 97–105.
[28] J. Wu, L. Yin, ACS Appl. Mater. Interface. 3 (2011) 4354–4362.
[29] E. Turkmen, S.Z. Bas, H. Gulce, S. Yildiz, Electrochim. Acta. 123 (2014) 93–102.
[30] H. Zhou, H. Chen, S. Luo, J. Chen, W. Wei, Y. Kuang, Biosens. Bioelectron. 20 (2005) 1305–1311.
[31] J. Chen, X. Zheng, Y. Li, H. Zheng, Y. Liu, S. Suye, J. Electrochem. Soc. 167 (2020) 067502.
[32] W. Zhang and G. Li, Third-generation biosensors based on the direct electron transfer of proteins. Analyt. Sci., 20(4), 603–609 | 10.2116/analsci.20.603, (accessed 16 April 2023).
[33] A. Şavk, H. Aydın, K. Cellat, F. Şen, J. Mol. Liq. 300 (2020) 112355.
[34] J.S. Narayanan, G. Slaughter, Bioelectrochemistry 128 (2019) 56–65.
[35] S.R. Chinnadayyala, I. Park, S. Cho, Microchimica. Acta. 185 (2018) 1–8.
[36] Y. Xie, T. Liu, Z. Chu, W. Jin, J. Electroanalyt. Chem. 893 (2021) 115328.
[37] Q. Dong, H. Ryu, Y. Lei, Electrochim. Acta. 370 (2021) 137744.
[38] X. Gao, X. Du, D. Liu, H. Gao, P. Wang, J. Yang, Scientif. Rep. 10 (2020) 1365, 2020 10:1.
[39] P.R. Nair, M.A. Alam, Phys. Rev. Lett. 99 (2007) 256101.
[40] P.R. Nair, M.A. Alam, Analyst 135 (2010) 2798–2801.
[41] P.R. Nair, M.A. Alam, Fractals 18 (2010) 461–476.
[42] P.R. Nair, M.A. Alam, Analyst 138 (2013) 525–538.
[43] D.A. Gough, J.Y. Lucisano, P.H.S. Tse, Anal. Chem. 57 (1985) 2351–2357.
[44] H. Yang, M.T. Rahman, D. Du, R. Panat, Y. Lin, Sens. Actuat. B. Chem. 230 (2016) 600–606.
[45] Y. Matsui, K. Hamamoto, Y. Kitazumi, O. Shirai, K. Kano, Analyt. Sci. 33 (2017) 845–851.
[46] C.P. McMahon, S.J. Killoran, R.D. O'Neill, J. Electroanalyt. Chem. 580 (2005) 193–202.
[47] D. Li, C. Batchelor-Mcauley, L. Chen, R.G. Compton, ACS Sens. 4 (2019) 2250–2266.
[48] J. Tsutsumi, A.P.F. Turner, W.C. Mak, Biosens. Bioelectron. 177 (2021) 112968.
[49] H. Park, P. Takmakov and H. Lee, *Sci. Rep.*, DOI:10.1038/S41598-018-22545-W.
[50] C. J. Bettinger, *Bioelectron. Med.*, DOI:10.1186/S42234-018-0007-6.
[51] K. Falconer, Fractal Geometry, 2nd edn., John Wiley & Sons, Ltd, 2003.
[52] S.R. Chinnadayyala, J. park, A.T. Satti, D. Kim, S. Cho, Electrochim. Acta. 369 (2021) 137691.
[53] T.T.-C. Tseng, H.G. Monbouquette, J. Electroanalyt. Chem. 682 (2012) 141–146.
[54] R. Aston, K. Sewell, T. Klein, G. Lawrie, L. Grøndahl, Eur. Polym. J. 82 (2016) 1–15.
[55] S. F. Cogan, https://doi.org/10.1146/annurev.bioeng.10.061807.160518, 2008, 10, 275–309.
[56] C. Boehler, S. Carli, L. Fadiga, T. Stieglitz, M. Asplund, Nat. Protocol. 15 (2020) 3557–3578. *2020 15:11*.
[57] Y.G. Zhou, Y. Wan, A.T. Sage, M. Poudineh, S.O. Kelley, Langmuir 30 (2014) 14322–14328.
[58] P. De Luna, S.S. Mahshid, J. Das, B. Luan, E.H. Sargent, S.O. Kelley, R. Zhou, Nano. Lett. 17 (2017) 1289–1295.
[59] S. Urban, A. Weltin, H. Flamm, J. Kieninger, B.J. Deschner, M. Kraut, R. Dittmeyer, G.A. Urban, Sens. Actuat. B. Chem. 273 (2018) 973–982.
[60] S.B. Hall, E.A. Khudaish, A.L. Hart, Electrochim. Acta. 43 (1998) 579–588.
[61] S.T. Larsen, M.L. Heien, R. Taboryski, Anal. Chem. 84 (2012) 7744–7749.
[62] J.J. Burmeister, G.A. Gerhardt, Anal. Chem. 73 (2001) 1037–1042.
[63] A. Weltin, K. Slotwinski, J. Kieninger, I. Moser, G. Jobst, M. Wego, R. Ehret, G. A. Urban, Lab. Chip. 14 (2014) 138–146.
[64] B. Wang, B. Koo, H.G. Monbouquette, Electroanalysis. 29 (2017) 2300–2306.
[65] X. Jin, T.S. Fisher, M.A. Alam, IEEE. Trans. Electron. Devices. 63 (2016) 4924–4932.
[66] M. Fratus, M.A. Alam, Biomed. Microdev. 26 (1) (2023) 4. Dec 14.
[67] I. Huang, M. Clay, S. Wang, Y. Guo, J. Nie, H.G. Monbouquette, Analyst. 145 (2020) 2602–2611.
[68] R. Madangopal, M. Stensberg, M. Porterfield, J. Rickus, N. Pulliam, 2012 IEEE Sensors, IEEE, 2012, pp. 1–4.
[69] J.C. Claussen, A. Kumar, D.B. Jaroch, M.H. Khawaja, A.B. Hibbard, D. M. Porterfield, T.S. Fisher, Adv. Funct. Mater. 22 (2012) 3399–3405.

Dr. Jian Xu received his post-doctorate degree from Weldon School of Biomedical Engineering at Purdue University in 2021. He received his M.E. and Ph.D. degrees in Mechanical Engineering from Stevens Institute of Technology in 2015 and 2019, respectively. His research focuses on the use of novel passive and active anti-biofouling strategies to extend the lifetime of implantable medical devices.

Marco Fratus received the B.Sc. (2014) and M.Sc. (2017) from Politecnico di Milano, Italy, in Biomedical and Electrical Engineering, respectively. He attended a Double M.Sc. degree (2015-2018) in Nanoelectronics at KTH, Sweden. As a Visiting Scholar at Columbia University, he investigated optoelectronic properties of graphene. His PhD research at Purdue University focuses on modeling, design, optimization of wearable and implantable electrochemical sensors.

Ankit Shah is a PhD student in Biomedical Engineering. He received his BS in Computer Science & Engineering from the University of New Mexico in 2021. He is currently pursuing PhD degree in biomedical engineering from Purdue University. He is interested in development of neural interface devices and its Brain Computer Interface applications. He wants to contribute particularly to the field of Dream Recording Technology and wearable neural devices for rehabilitation.

James K. Nolan received his PhD degree in Biomedical Engineering at Purdue University, West Lafayette, IN, USA, where we received a B.S. Biological Engineering and M.S. in Agricultural and Biological Engineering. His research interests include electrochemical biosensors for neurotransmitters and metabolic markers, applied to wearable devices, implantable devices, and microphysiometry.

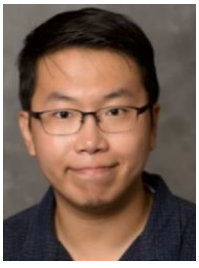

Jongcheon Lim received his PhD degree in biomedical engineering from Purdue University in 2023. He had received the B. S. degree in materials science & engineering from Yonsei University, Seoul, South Korea in 2015, the M.S. degree in bio & brain engineering from Korea Advanced Institute of Science and Technology (KAIST), Daejeon, South Korea in 2017. He is currently pursuing PhD degree in biomedical engineering from Purdue University, West Lafayette, IN, USA. His research interest includes implantable biosensors, microfabricated neural interface devices and soft implantable materials.

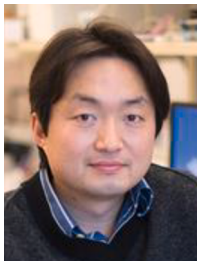

Prof. Chi Hwan Lee is the Lesli A. Geddes Associate Professor of Biomedical Engineering and Associate Professor of Mechanical Engineering, and by Courtesy, of Materials Engineering and Speech, Language, and Hearing Sciences at Purdue University. He received M.S. and Ph.D. degrees in Mechanical Engineering from Stanford University in 2009 and 2013, respectively. Prior to joining Purdue in 2015, he was a postdoctoral research associate in Department of Materials Science and Engineering at University of Illinois at Urbana-Champaign under the guidance of Professor John A. Rogers. His scholarly efforts are dedicated to addressing unmet clinical needs using novel yet simple wearable devices with a clear path towards translation to produce measurable clinical and economic impacts.

Prof. Muhammad Ashraful Alam (M'96–SM'01–F'06) received the Ph.D. degree from Purdue University, West Lafayette, IN, USA, in 1995. After a decade at Bell Laboratories, he returned to Purdue in 2004, where he currently holds the Jai N. Gupta Professorship of Electrical Engineering. His research includes physics, performance limits, and novel concepts in biosensors, solar cells, and transistors.

Prof. Hyowon "Hugh" Lee is an associate professor of Biomedical Engineering at Purdue University. He received his M.S. and Ph.D. degrees in Biomedical Engineering from the University of California, Los Angeles, in 2008 and 2011, respectively. Before joining Purdue, he worked as a senior engineer for St. Jude Medical's Implantable Electronic Systems Division where he worked on manufacturing challenges associated with implantable electronic devices such as pacemakers, implantable cardioverter defibrillators, deep brain stimulators, and spinal cord stimulators. His current research interest centers around improving the reliability and the functionality of implantable sensors and actuators toward building smarter medical devices.